Journal of Power Sources 195 (2010) 1211–1215

Contents lists available at ScienceDirect

Journal of Power Sources

journal homepage: www.elsevier.com/locate/jpowsour

Short communication

Synthesis of $LiFePO_4$/polyacenes using iron oxyhydroxide as an iron source

Guiling Yang[a,b], Xianfa Zhang[a,b], Jing Liu[a,b], Xingguang He[a,b], Jiawei Wang[a,b], Haiming Xie[a,b], Rongshun Wang[a,b,*]

[a] Institute of Functional Materials, Department of Chemistry, Northeast Normal University, Changchun, Jilin 130024, PR China
[b] LIB Engineering Laboratory, Materials Science and Technology Center, Changchun, Jilin 130024, PR China

ARTICLE INFO

Article history:
Received 16 June 2009
Received in revised form 22 August 2009
Accepted 24 August 2009
Available online 31 August 2009

Keywords:
Lithium iron phosphate
Iron oxyhydroxide
Cathode
Mechanism
Lithium ion batteries

ABSTRACT

$LiFePO_4$/polyacenes (PAS) composite is synthesized by iron oxyhydroxide as a new raw material and phenol–formaldehyde resin as both reducing agent and carbon source. The mechanism of the reaction is outlined by the analysis of XRD, FTIR as well as TG/DSC. The results show that the formation of $LiFePO_4$ is started at 300 °C, and above 550 °C, the product can be mainly ascribed to olivine $LiFePO_4$. The electrochemical properties of the synthesized composites are investigated by charge–discharge tests. It is found that the prepared sample at 750 °C (S750) has a better electrochemical performance than samples prepared at other temperatures. A discharge capacity of 158 mAh g^{-1} is delivered at 0.2 C. Under high discharge rate of 10 C, a discharge capacity of 145 mAh g^{-1} and good capacity retention of 93% after 800 cycles are achieved. The morphology of S750 and PAS distribution in it are investigated by SEM and TEM.

1. Introduction

Since lithium iron phosphate as a promising cathode material for lithium ion batteries was first reported in 1997 [1], it has been well known as a promising cathode material for lithium ion batteries in applications such as power tools, electric vehicles (EVs) and hybrid electric vehicles (HEVs), due to its safety, environmental benign, and relatively low cost [2,3], and great efforts have been devoted to improve the electrochemical performances. Although enhanced performances have been obtained by different synthesis routes such as sol–gel methods, coprecipitation and hydrothermal processes [4–7], many obstacles have been encountered for these methods from a laboratory process to mass production because of the complicated synthesis techniques and the hard controlled synthesis situation. Solid-state reaction is still the better choice.

Solid-state preparative approaches had relied on the use of Fe^{2+} precursor compounds, typically iron (II) oxalate [1,8], or iron (II) acetate [9]. Apart from being expensive, the multistage preparative strategies are not considered commercially favorable. Since J. Barker [10] applied a carbothermal reduction (CTR) technique as a convenient and energy efficient method to synthesize $LiFePO_4$ from Fe^{3+} precursor, iron (III) compounds such as cheap Fe_2O_3 [10–12] or $FePO_4$ [7,13,14] have been considered a lot in recent reports.

As one of the iron (III) compounds, iron oxyhydroxide (FeOOH) has been extensively used in the production of pigment, catalysts, raw materials of hard and soft magnets, because it is inexpensive and abundant. Recently, FeOOH has been investigated as cathode materials in Li-ion batteries [15–18]. However, to the best of our knowledge, its application as an iron precursor in the preparation of $LiFePO_4$ has not been reported.

Herein, we have attempted to synthesize $LiFePO_4$/PAS composite by using FeOOH as a novel Fe (III) raw material, and PF resin as both a reducing agent and carbon source. Moreover, the reaction mechanism has been explored and the electrochemical performance of the as-prepared $LiFePO_4$/PAS is investigated. In addition, PAS as one of the conductive carbons pyrolyzed from PF resin [19,20] to improve the performance of $LiFePO_4$ have been reported by our group [21,22].

2. Experimental

The $LiFePO_4$/PAS samples were synthesized from FeOOH, LiH_2PO_4 and phenol–formaldehyde (PF) resin as starting materials. Stoichiometric amounts of FeOOH, LiH_2PO_4 and suitable amounts of PF resin (ca. 10–15 wt.%) were mixed in ethanol. After ball milling, the mixed slurry was dried in an oven. Finally, the resulting precursor was heated in a tube furnace to get the samples at 300, 350, 400, 450, 550, 600, 675, 750 °C for 8 h under N_2 atmosphere. They are denoted as S300, S350, S450, S550, S600, S675, S750, respectively.

The carbon content in the sample was determined by the VarioEL III (Elementar, Germany). The thermal behavior of precursor was concerned with the Thermogravimetric-differential scanning

* Corresponding author at: Institute of Functional Materials, Department of Chemistry, Northeast Normal University, Renmin Street 5268, Changchun, Jilin 130024, PR China. Tel.: +86 0431 85099511; fax: +86 0431 85099511.
E-mail address: wangrs@nenu.edu.cn (R. Wang).

0378-7753/$ – see front matter © 2009 Elsevier B.V. All rights reserved.
doi:10.1016/j.jpowsour.2009.08.060

calorimetry (TG/DSC) apparatus (Pyris Diamond, PerkinElmer Thermal Anylysis) under nitrogen flow. The sample was heated from ambient to 800 °C at the rate of 10 °C min^{-1}. In order to analyze the crystalline structure of the prepared samples, X-ray diffraction (XRD) was performed with a Rigaku P/max 2200VPC using a Cu K(radiation source (λ = 1.5406 Å) by a powder diffraction method. FTIR analysis was performed on KBr-supported samples using a Magna 560 spectrometer (American Nicolet). FEG XL-30 SEM and JEOL-JEM-2010 TEM were used to observe the particle size and morphology of the samples. After the powder samples were pressed in the form of disks at 12 MPa, typically with a diameter of 15 mm and a thickness of 1–3 mm, four-point probe meter (SDY-5) was used to measure the electronic conductivity of the samples.

The performance of the $LiFePO_4$ as cathode was evaluated using a coin-type cell (size 2025) with a lithium metal anode. The working electrode was made by dispersing 80 wt.% active materials ($LiFePO_4$/PAS), 10 wt.% carbon black, and 10 wt.% polyvinylidene fluoride (PVDF) binder in N-methylpyrrolidone (NMP) solvent to form a homogeneous slurry. The slurry was then spread on Al foil. The coated electrodes were dried in vacuum at 120 °C for 12 h. The cells were assembled in an argon atmosphere filled glove box. The electrolyte was 1 M $LiPF_6$ in a mixture of ethylene carbonate (EC) and dimethyl carbonate (DMC) (1:1 volume). The cells were galvanostatically charged and discharged between 2.0 and 4.2 V versus Li/Li^+ at room temperature on the electrochemical test instrument (CT2001A, Wuhan Land Electronic Co. Ltd., China), 1 C = 170 mA g^{-1}.

3. Results and discussion

3.1. Thermal analysis

The TG/DSC curves for the mixture of the precursor are presented in Fig. 1. Under the N_2 atmosphere, there are several stages of weight loss in the TG plot and both endothermic and exothermic peaks in the DSC plot. Around 210 °C, an initial weight loss and an endothermic peak appear. This corresponds to the elimination of structural water of FeOOH [15] and should also be related to the lost of water of LiH_2PO_4 to form a dimer ($Li_2H_2P_2O_7$) [8]. In the region from 300 to 450 °C, the broad exothermic peak and the continuous weight loss could be related to the combination of the reactants to form lithium iron phosphate ($LiFePO_4$) and a side reaction to form $LiFeP_2O_7$. As the temperature increases above 450–500 °C, a small second exothermic peak is observed, this is probably corresponding to the reduction of $LiFeP_2O_7$ to $LiFePO_4$ (Eq. (7)). From 500 to 800 °C,

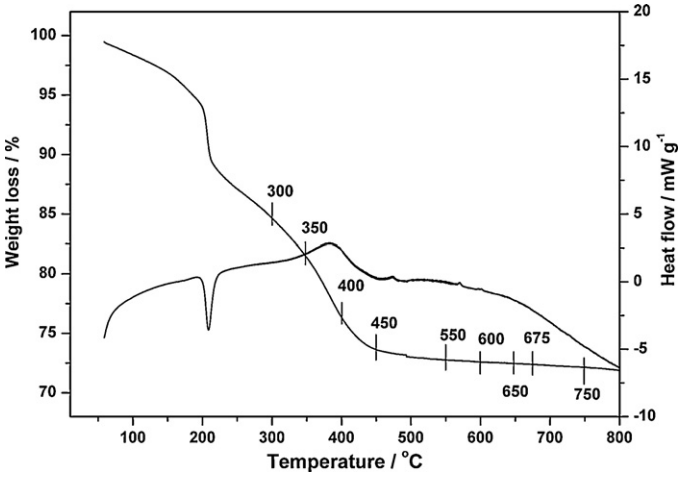

Fig. 1. The TG/DSC curves for the mixture of the precursor. The vertical symbols and the marked numbers on the TG curve indicate the sintering temperatures of the samples.

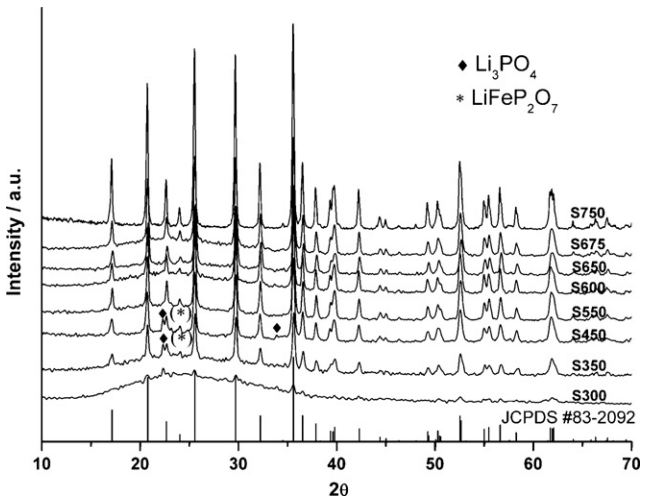

Fig. 2. The XRD spectra of the samples LFP sintered for 8 h at 300–750 °C.

the resulting precursor kept a very slow weight loss, the behavior is probably associated with the further pyrolysis of PF resin in the N_2 flow.

The above reaction involved may be summarized as following:

Around 210 °C:

$$FeOOH\,xH_2O \rightarrow FeOOH + xH_2O \quad (1)$$

$$2LiH_2PO_4 \rightarrow Li_2H_2P_2O_7 + H_2O \quad (2)$$

At 300–450 °C:

$$LiH_2PO_4 + FeOOH + RE \rightarrow LiFePO_4 \quad \text{(main reaction)} \quad (3)$$

$$Li_2H_2P_2O_7 + FeOOH \rightarrow LiFeP_2O_7 + LiOH + H_2O \quad \text{(side reaction)} \quad (4)$$

$$2LiOH + LiH_2PO_4 \rightarrow Li_3PO_4 + H_2O \quad \text{(sides reaction)} \quad (5)$$

$$FeOOH + RE \rightarrow Fe_3O_4 + H_2O \quad \text{(side reaction)} \quad (6)$$

At 450 to 500 °C:

$$2LiFeP_2O_7 + Li_3PO_4 + Fe_3O_4 + RE \rightarrow 5LiFePO_4 \quad \text{(side reaction)} \quad (7)$$

(RE = reducing agent)

where RE represents the reducing agents in the synthesis process, and it is some reducing gases such as H_2 or gaseous hydrocarbons evolved during the calcinations of the PF resin [14].

3.2. XRD analysis

The different stages of the $LiFePO_4$ synthesis are illustrated in Fig. 2. The patterns of the samples sintered at the temperature range are actually dominated by the pattern characteristics of $LiFePO_4$. In the early stages, the Bragg peaks of $LiFePO_4$ emerge from the amorphous background at 300 °C, giving evidence that the $LiFePO_4$ formation has just started at this temperature. As the temperature increases, the intensity is strengthened. It shows that more quantity of $LiFePO_4$ is crystallized. The XRD signal at around 2θ = 23.3 and 40° reflects detectable amounts of $LiFeP_2O_7$ and Li_3PO_4 phases appeared in the sample. Above 550 °C, the impurity phase is disappeared, and all diffraction peaks can be attributed to an ordered olivine $LiFePO_4$ structure, indicating that $LiFeP_2O_7$ is reduced to $LiFePO_4$. In the range of 550–750 °C, the peaks gradually sharpen

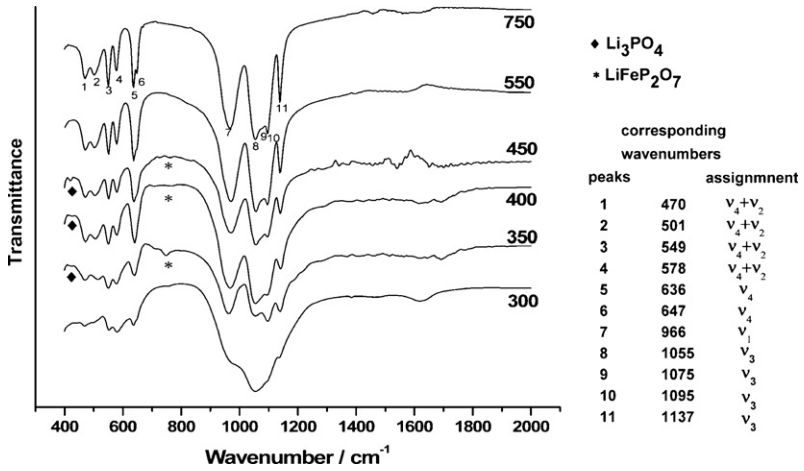

Fig. 3. The FTIR spectroscopy of the samples calcined at different temperatures in the range of 300–750 °C.

with the increasing temperature, indicating that an increase of crystallinity as may occur from growth of grain size, ordering of local structure, and release of lattice strain [8].

3.3. FTIR spectroscopy

As shown in Fig. 3, plot 750 is composed of both PAS and $LiFePO_4$ characteristic peaks. The numbered peaks are all indexed with the vibration of olivine lithium iron phosphate [23], and the weak peaks in the region of 1400–1600 cm^{-1} are corresponding to the absorbance of the residual carbon [22]. And from plot 300 to plot 550, the bands of weak intensity in the spectral range from 1300 to 1800 cm^{-1} are corresponding to the incompletely pyrolytic product of PF resin at the temperature range of 300–550 °C [22].

As analyzed in the XRD patterns, in the early stage of the synthesis, olivine $LiFePO_4$ starts to form at 300 °C. At this temperature, the IR bands are very broad, confirming that LFP particles are of poor crystallinity. As the temperature increases, the spectrum becomes better resolved. This shows that the $LiFePO_4$ materials synthesized at higher temperatures have better crystalline olivine structure. The asterisks and the black diamonds in the plots indicate the impurities such as Li_3PO_4 and $LiFeP_2O_7$ exist in the samples prepared at low temperature from 350 to 450 °C. In sample S550, all absorbance bands can be ascribed to the vibration of olivine $LiFePO_4$ in the region of 1400–1700 cm^{-1}. Combined with the TG/DSC and XRD analysis, it indicates that the iron (III) compounds such as the observed $LiFeP_2O_7$ is reduced, and Li_3PO_4 is one reactant in the reaction (Eq. (7)). This was in correspondence with TG/DSC and the XRD analysis above.

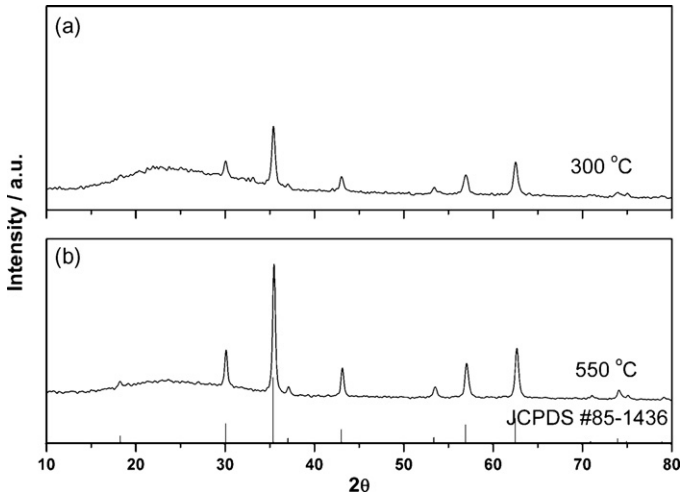

Fig. 4. XRD patterns of the FeOOH mixed with 10% PF resin sintered at 300 and 550 °C under N_2 flow.

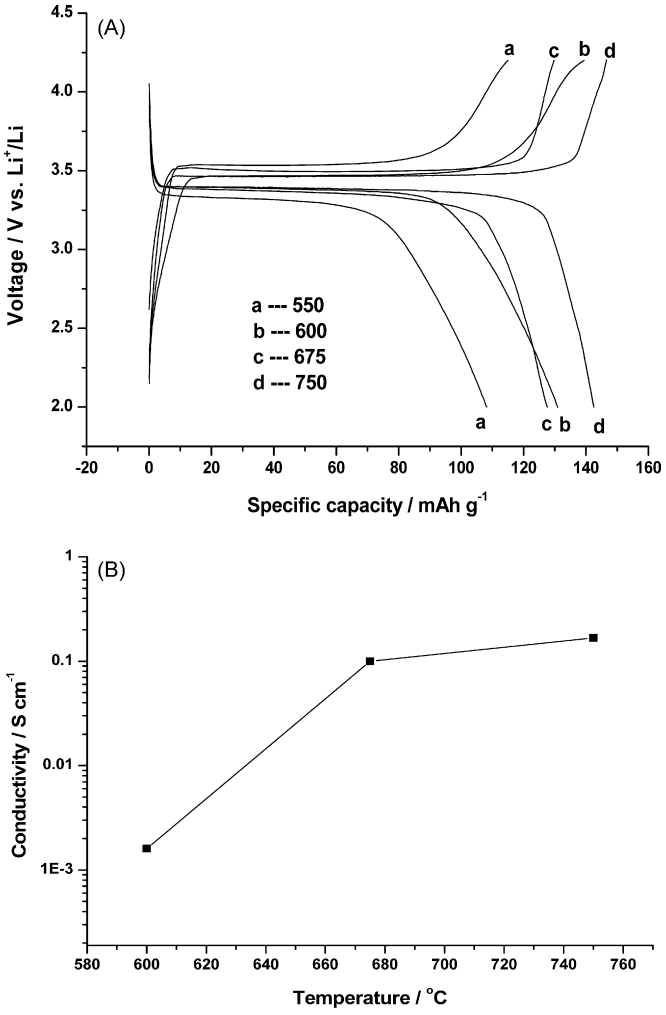

Fig. 5. (A) Charge–discharge curves of $LiFePO_4$/PAS samples treated to different temperatures (indicated within the labels). In all cases, the current was set to 0.5 C (ca. 34 mA g^{-1}). (B) Development of electric conductivity with temperature of sample treatment.

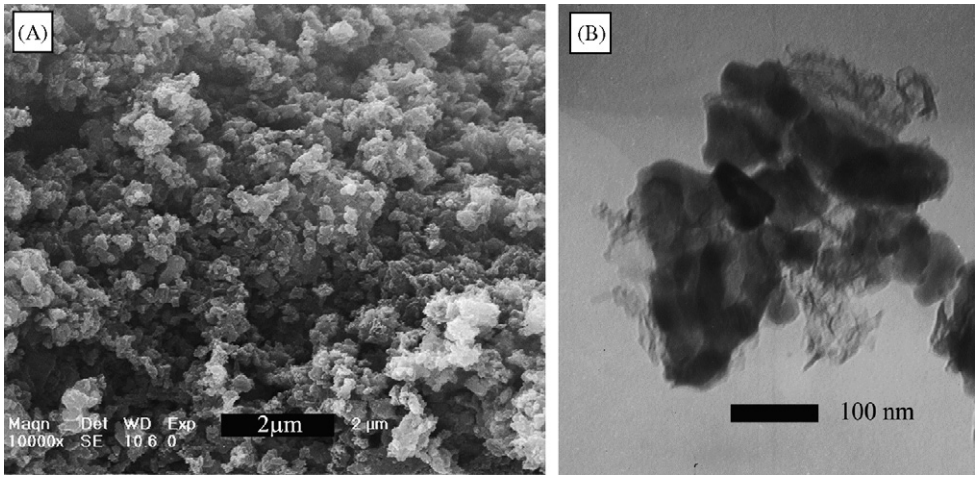

Fig. 6. SEM image (A) and TEM image (B) of S750.

Although FTIR measurements and X-ray diffractometry are not sensitive to detect of low concentrations of impurities (at the ppm level) [24], we can conclude that there is no large quantity of iron oxide formed during the early synthesis.

To investigate the reaction of FeOOH under the reductive atmosphere, we evaluated the products synthesized from FeOOH mixed with PF resin at 300 and 550 °C. As shown in Fig. 4, the XRD patterns show that under the condition with PF resin providing the reductive atmosphere, FeOOH is likely to transform to Fe_3O_4 rather than Fe_2O_3. Based on the analysis above, we deduce that $LiFeP_2O_7$ and Li_3PO_4 will react with Fe_3O_4 to form $LiFePO_4$, as shown in Eq. (7). No character peaks of Fe_3O_4 appears in the XRD patterns of the samples from plot 300 to plot 750, indicating its small quantity in the preparation process.

3.4. Electrochemistry of $LiFePO_4$/PAS composite synthesized at different temperatures

Galvanostatic testing of the material above 550 °C (Fig. 5) shows the electrochemical performance of the samples prepared at different temperatures under the discharge rate of 0.2 C. The best result is obtained at 750 °C. As shown in plot d of Fig. 5A, a flat and long charge and discharge voltage plateau is located at 3.46 and 3.39 V and a capacity of 142 mAh g^{-1} is delivered. The reasons for the increase in capacity are associated with the increase of the electronic conductivity, as shown in Fig. 5B, and the better crystallinity as mentioned above. The performance of the samples sintered at higher temperatures than 750 °C are not discussed in this paper, because it is more energy consuming, and the related reports indicate that the capacities will decrease due to the agglomeration of the small particles into larger ones and the impurities appeared [8,9,25].

3.5. Morphology of $LiFePO_4$/PAS synthesized at 750 °C

The morphology of $LiFePO_4$/PAS prepared under the optimized temperature (750 °C) is described in Fig. 6. Fig. 6A represents the S750 materials consisting of nanometric lithium iron phosphate particles with an irregular morphology partially or fully fused together into larger agglomerates. The morphology of the existed PAS cannot be observed obviously by SEM and in order to verify its distribution in the powders, TEM images were illustrated in Fig. 6B. It can be seen that PAS distributes between the particles, and it is not likely that it coats all the particles evenly in the sample. However, as a conductive carbon, PAS between the particles contribute to the enhanced electronic conductivity.

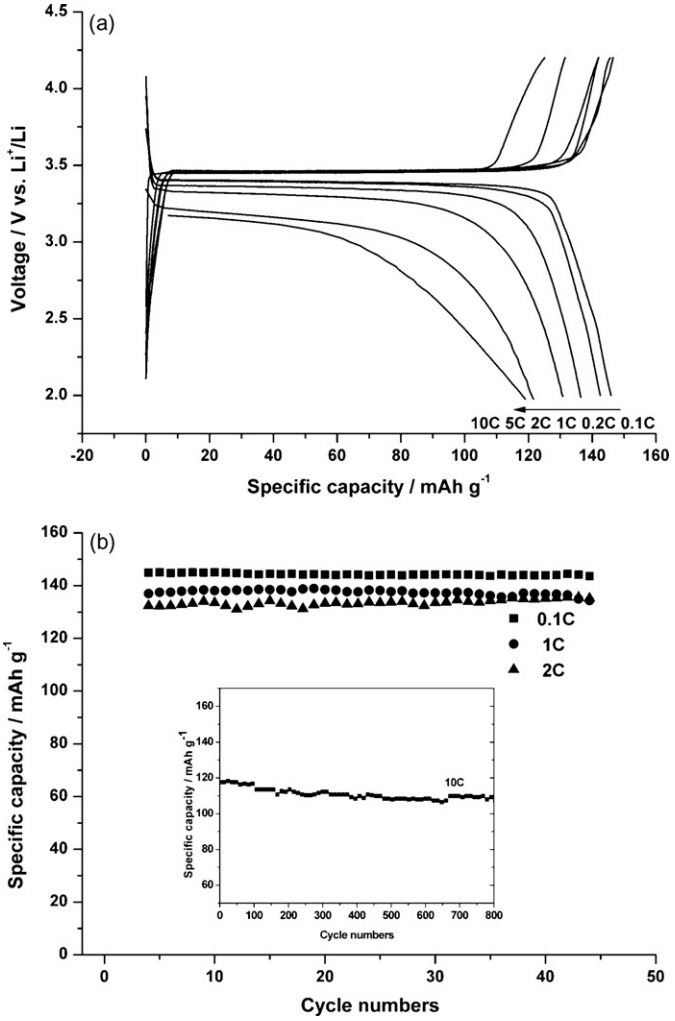

Fig. 7. (a) Charge–discharge profiles of S750 at different currents rates. (b) Discharge capacity versus cycle number at room temperature from 0.1 to 2 C. The inset is cycling performance of S750 at 10 C for 800 cycles.

Table 1
The capacity of S750 and the corresponding capacity of $LiFePO_4$ when neglecting the residual inert carbon of it at different discharging rate.

The discharging rate	0.2 C (34 mA g^{-1})	1 C (170 mA g^{-1})	5 C (850 mA g^{-1})	10 C (1700 mA g^{-1})
The capacity of the $LiFePO_4$/PAS composite (mAh g^{-1})	143	136	122	118
The capacity of the $LiFePO_4$ (mAh g^{-1})	158 (93% DOD)	151 (89% DOD)	136 (80% DOD)	131 (77% DOD)

In addition, the depth of discharge (DOD) at the end of the fully discharge is 100% DOD.

3.6. Electrochemical performance of $LiFePO_4$/PAS synthesized at 750 °C

The electrochemical rate performance and cyclability of S750 are shown in Fig. 7. The discharge capacities are 143 mAh g^{-1} at 0.2 C, and the voltage profile exhibits very flat plateaus, which indicates that the two-phase redox reaction proceeds via a first-order transition between $LiFePO_4$ and $FePO_4$. Under higher currents, the capacities are certain to decrease, but a capacity of 136, 131, 118 mAh g^{-1} can still be delivered at the rate of 1, 2 and 10 C, respectively. The capacity retention is very good at low current rates after 40 cycles. At the high current of 10 C, the capacity retention is 93% after 800 cycles, indicating a promising cycling performance.

The residual conductive carbon is intrinsically an inert material for Li^+ storage, and the increasing amount of carbon as the active material would certainly lead to capacity loss. Table 1 gives the discharge capacity values observed and the value calculated when the inert carbon (10 wt.%) is ignored for the $LiFePO_4$/PAS composite S750. The capacities would be 158, 151, 146 and 137 mAh g^{-1} at 0.2, 1, 2 and 5 C, respectively, as the carbon (PAS) is neglected in the $LiFePO_4$PAS composite, as shown in Table 1.

4. Conclusions

In this paper, lithium iron phosphate was successfully synthesized from iron oxyhydroxide, which is an abundant and inexpensive iron source. During the heating process, $LiFePO_4$ starts to form at 300 °C and above 550 °C, all X-ray diffraction peaks of the products can be attributed to an ordered olivine $LiFePO_4$ structure. The peaks gradually sharpen with the increasing temperature, which indicates the increase of crystallinity. The results are in correspondence with TG/DSC and IR analysis.

The electrochemical properties of the synthesized composite are investigated, and S750 has a better electrochemical performance than samples prepared at other temperatures. An initial capacity of 158 mAh g^{-1} is obtained at 0.2 C and excellent high-rate performance is also achieved. The good electrochemical performance demonstrates that the route is promising to synthesize $LiFePO_4$ as the cathode material in lithium ion batteries.

Acknowledgement

This work was supported by the project of the Science and Technology development Program of Jilin Province (Grant Nos. 20076020, 20080304).

References

[1] A.K. Padhi, K.S. Nanjundaswamy, J.B. Goodenough, J. Electrochem. Soc. 144 (1997) 1188–1194.
[2] S.I. Nishimura, G. Kobayashi, K. Ohoyama, R. Kanno, M. Yashima, A. Yamada, Nat. Mater. 7 (2008) 707–711.
[3] S.Y. Chung, J.T. Bloking, Y.M. Chiang, Nat. Mater. 1 (2002) 123–128.
[4] R. Dominko, M. Bele, J.M. Goupil, M. Gaberscek, D. Hanzel, I. Arcon, J. Jamnik, Chem. Mater. 19 (2007) 2960–2969.
[5] C. Delacourt, P. Poizot, S. Levasseur, C. Masquelier, Electrochem. Solid-State Lett. 9 (2006) A352–A355.
[6] Z. Wang, S. Su, C. Yu, Y. Chen, D. Xia, J. Power Sources 184 (2008) 633–636.
[7] Y.G. Wang, Y.R. Wang, E. Hosono, K.X. Wang, H. Zhou, Angew. Chem. Int. Ed. 47 (2008) 7461–7465.
[8] S.S. Zhang, J.L. Allen, K. Xu, T.R. Jow, J. Power Sources 147 (2005) 234–240.
[9] A. Yamada, S.C. Chung, K. Hinokuma, J. Electrochem. Soc. 148 (2001) A224–A229.
[10] J. Barker, M.Y. Saidi, J.L. Swoyer, Electrochem. Solid-State Lett. 6 (2003) A53–A55.
[11] C.W. Kim, J.S. Park, K.S. Lee, J. Power Sources 163 (2006) 144–150.
[12] H. Liu, D. Tang, Solid State Ionics 179 (2008) 1897–1901.
[13] L.N. Wang, Z.G. Zhang, K.L. Zhang, J. Power Sources 167 (2007) 200–205.
[14] N. Ravet, M. Gauthier, K. Zaghib, J.B. Goodenough, A. Mauger, F. Gendron, C.M. Julien, Chem. Mater. 19 (2007) 2595–2602.
[15] C. Benoit, C. Bourbon, P. Berthet, S. Franger, J. Phys. Chem. Solids 67 (2006) 1265–1269.
[16] K. Amine, H. Yasuda, M. Yamachi, J. Power Sources 81/82 (1999) 221–223.
[17] G. Jain, C.J. Capozzi, J.J. Xu, J. Electrochem. Soc. 150 (2003) A806–A810.
[18] H.F. Shao, X.F. Qian, J. Yin, Z.K. Zhu, J. Solid State Chem. 178 (2005) 3130–3136.
[19] K. Tanaka, K. Ohzeki, T. Yamabe, Synth. Metals 9 (1984) 41–52.
[20] K. Tanaka, A. Ito, T. Yoshii, S. Suehiro, S. Nagura, N. Ando, Y. Hato, Carbon 39 (2001) 1599–1603.
[21] G.L. Yang, A.F. Jalbout, Y. Xu, H.Y. Yu, X.G. He, H.M. Xie, R.S. Wang, Electrochem. Solid-State Lett. 11 (2008) A125–A128.
[22] H.M. Xie, R.S. Wang, J.R. Ying, et al., Adv. Mater. 18 (2006) 2609–2613.
[23] C.M. Burba, R. Frech, J. Electrochem. Soc. 151 (2004) A1032–A1038.
[24] K. Zaghib, N. Ravet, M. Gauthier, F. Gendron, A. Maugere, J.B. Goodenough, C.M. Julien, J. Power Sources 163 (2006) 560–566.
[25] S.J. Kwon, C.W. Kim, W.T. Jeong, K.S. Lee, J. Power Sources 137 (2004) 93–99.